

Chapter 22

Atmospheric Coupling by Gravity Waves: Climatology of Gravity Wave Activity, Mesospheric Turbulence and Their Relations to Solar Activity

Werner Singer, Peter Hoffmann, G. Kishore Kumar, Nicholas J. Mitchell,
and Vivien Matthias

Abstract Gravity waves (GW) are important for the coupling between the different regions of the middle atmosphere. They are normally generated in the troposphere, are filtered by the wind field in the stratosphere and lower mesosphere and dissipate at least partly in upper mesosphere and lower thermosphere (MLT). The activity of gravity waves, their filtering by the mean circulation, and the variation of GW activity with solar activity have been studied using long-term wind measurements with Medium Frequency (MF) radars and meteor radars at high and middle northern latitudes. The GW activity is characterized by a semi-annual variation with a stronger maximum in winter and a weaker in summer consistent with the selective filtering of westward and eastward propagating GWs by the mean zonal wind. The latitudinal variation of GW activity shows the largest values in summer at mid-latitudes between 65 km and 85 km accompanied with an upward shift of the height of wind reversal towards the pole. Long-term observations of the MLT winds at mid latitudes indicate a stable increase of westward directed winds below about 85 km and an increase of eastward directed winds above 85 km especially during summer. The observed long-term trend of zonal wind at about 75 km goes along with an enhanced activity of GWs with periods of 3 to 6 hours at altitudes between 80 km and 88 km. In addition, the mesosphere responds to severe solar proton events (SPE) with increased eastward directed winds above about 85 km. The vertical coupling from the troposphere up to the lower thermosphere due to gravity waves and planetary waves is discussed for major sudden stratospheric warmings (SSW) for the winters 2006 and 2009.

W. Singer (✉) · P. Hoffmann · G. Kishore Kumar · V. Matthias
Leibniz-Institute of Atmospheric Physics at the Rostock University, Schlosstr. 6, 18225
Kühlungsborn, Germany
e-mail: singer@iap-kborn.de

P. Hoffmann
e-mail: hoffmann@iap-kborn.de

N.J. Mitchell
Centre for Space, Atmospheric and Oceanic Science, Department of Electronic and Electrical
Engineering, University of Bath, Claverton Down, Bath BA2 7AY UK
e-mail: N.J.Mitchell@bath.ac.uk

22.1 Introduction

During recent years the middle atmosphere (10 to 110 km) has been recognized as an essential part of the climate system. The natural internal variability of the climate and its sensitivity to perturbations can only be understood when the middle atmosphere is taken into account. The mesosphere (50 to 100 km) is of particular importance because both short-term and long-term variations exceed those in the troposphere (0–10 km) by an order of magnitude. To understand the general structure and dynamics of the atmosphere and its variability it is important to know the coupling between different atmospheric regions from the troposphere up to the thermosphere. Often changes caused by solar or non-solar sources are observed at height regions which could be different from the origin of this effect. Important coupling processes are radiative exchanges, transport of chemically active minor constituents and dynamical processes. The dynamical coupling mainly includes forcing of different atmospheric waves (GW, tides, and planetary waves), their propagation through the atmosphere, the interaction between different waves and their impact upon the mean circulation. The dynamical coupling is considered to be the most important aspect of atmospheric coupling. Here especially the gravity waves play an essential role.

Starting with the basic study of *Hines* [1960], many experimental and theoretical investigations have been carried out concerning different aspects of GW sources, propagation, interaction with other waves and the mean circulation, and their dissipation and the creation of turbulence. Excellent reviews of the most important results have been given by *Fritts* [1984] and *Fritts and Alexander* [2003]. As most important GW sources have been detected: topographic generation [e.g., *Nastrom and Fritts*, 1992], convection events [mainly in the tropics, e.g., *Vincent and Alexander*, 2000], frontal systems and jet streams [*Fritts and Nastrom*, 1992]. A survey on the characteristics and influences arising from various GW sources was given by *Fritts et al.* [2006]. The propagation of GW is mainly controlled by the atmospheric wind field. For the normal case of tropospheric sources the GW spectrum in the mesopause region depends markedly on the filtering effect of the wind field in the strato- and mesosphere [*Lindzen*, 1981] due to reflection and absorption of GW at critical levels. Therefore, the observed GW signatures observed in the MLT region contain information about their sources and also about the wind field between the source and the observing region.

The chapter is organized as follows: In Sect. 22.2 our data base and methods are described. Long-term variations of winds and GWs are presented in Sect. 22.3. Our results of vertical coupling processes during SSWs are summarized in Sect. 22.4, whereas Sect. 22.5 presents the responses of the MLT wind field on SPE. Finally, the main results are summarized in Sect. 22.6.

22.2 Experimental Techniques

Continuous measurements of winds in the mesosphere and lower thermosphere as well as temperatures around the mesopause have been carried out with MF radars

Table 22.1 Technical details of the MF and meteor radars at Juliusruh and Andenes

	Juliusruh 55°N, 13°E		Andenes 69°N, 16°E		MF Doppler
	MF	Meteor	MF	Meteor	
Frequency	3.18 MHz	32.55 MHz	1.98 MHz	32.55 MHz	3.17 MHz
Beam width	~15°	All-sky <60°	~60°	All-sky <60°	6.4°
Pulse length	27 μs	13 μs	27 μs	13 μs	10 μs
Sampling res.	2 km	2 km	2 km	2 km	1 km
Height range	70–94 km	80–100 km	70–94 km	80–100 km	60–94 km
Parameters	winds (FCA)	winds (Doppler)	winds (FCA)	winds (Doppler)	electron density, Doppler winds, turbulence
Observations since	1990–	1999–2001 2007–	1998–	2001– Kiruna: 1999–	2003–

and meteor radars at Andenes (69°N, 16°E), and Juliusruh (55°N, 13°E). The basic parameters of the radars are summarized in Table 22.1. Winds from the MF radars at Juliusruh (3.18 MHz) and Andenes (1.98 MHz) are determined by the spaced-antenna method [e.g., *Briggs, 1984*], details about these radars are given by *Singer et al. [1997]*, *Keuer et al. [2007]* and *Hoffmann et al. [2011]*.

The all-sky meteor radars at Andenes and Juliusruh are classical meteor radars [e.g., *Hocking et al., 2001*; *Singer et al., 2003*]. From each meteor the radial velocity of the meteor trail due to its movement with the background wind is estimated. The data are binned in height intervals of 3 km and time intervals of one hour to determine horizontal winds between 82 and 98 km. Furthermore, at the peak of the meteor layer at about 90 km (for 32.55 MHz) daily mean temperatures were derived from the height variation of the meteor decay time in combination with an empirical model of the mean temperature gradient at the peak altitude [for details see *Singer et al., 2004*; *Hocking et al., 2004*].

The acquired time series from the MF and meteor radars with lengths up to 20 years allow studies of possible trends and solar cycle variations of the wind field in the MLT region. Prevailing winds as well as diurnal and semidiurnal tides are obtained from harmonic analysis of a sliding 4-day composite of hourly winds for each radar [e.g. *Singer et al., 2005*]. If available, we combine the winds obtained by the MF radars from 70–82 km and meteor radars from 82–95 km to get reliable winds over an extended altitude range from 70–95 km at Andenes and Juliusruh [see also *Hoffmann et al., 2007, 2010*]. The advantages of this method are obvious when comparing both panels in Fig. 22.1, showing an excellent agreement between both data sets at 82–84 km, but also indicating differences at altitudes above 85 km where the MF radar winds tend to be smaller than those recorded by the meteor radars. This is in agreement with earlier works showing MF radar winds above about 85 km were weak compared with winds measured by the UARS satellite [e.g. *Burrage et al., 1996*]. Monthly medians of prevailing winds and tides are used for time series

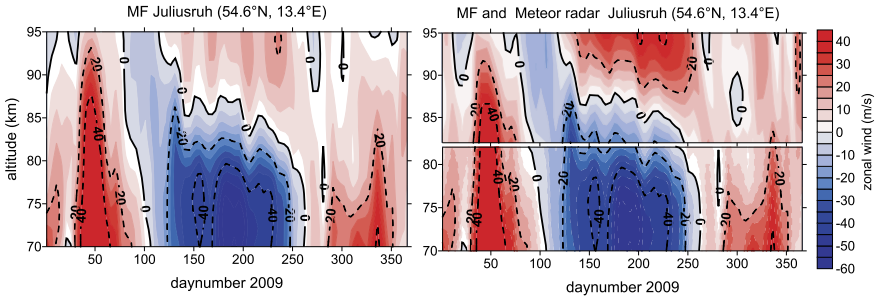


Fig. 22.1 Mean zonal winds observed at Juliusruh in 2009. *Left panel:* MF radar winds (70–95 km); *Right panel:* combined MF radar (70–82 km) and meteor radar (82–95 km) winds

analysis, as medians are outlier-resistant [e.g. *Weatherhead et al., 1998*]. Ground-based and satellite observations of tidal signatures in the MLT region during the CAUSES tidal campaigns showed that satellite and ground-based tidal characteristics are in good agreement and it could be proved for the first time that both types of observations are consistent with each other [e.g., *Ward et al., 2010*].

Additional parameters, e.g. turbulence and electron density used in Sects. 22.4 and 22.5, were derived with the narrow beam Saura MF Doppler radar [*Latteck et al., 2005; Singer et al., 2008, 2011*].

22.3 Climatology of Winds and Gravity Wave Activity

22.3.1 Trends and Solar Cycle Variation of Mean Winds

Ten years of meteor wind observations at Andenes cover nearly a complete solar cycle. The data base could be extended to a full solar cycle adding the meteor radar observations from Kiruna, Sweden [*Mitchell et al., 2002*] for the period August 1999 to August 2001. Both systems (270 km apart) use identical radar technology and a comparison of the wind measurements demonstrated that both sites give representative information about the MLT dynamics over northern Scandinavia [*Pancheva et al., 2007*]. The extended data set has been used to get an initial estimate of possible trends and solar activity variations of the MLT wind field although longer time series would be preferable for a reliable separation of solar activity influence and trend. The seasonal variation of the zonal mean wind for the period 1999 to 2010 is dominated by the persistent feature of a strong westward directed jet below about 88 km and an eastward directed jet above that altitude in summer (Fig. 22.2).

The wind field is subject to strong variability in winter due to planetary waves and associated sudden stratospheric warmings (see also Sect. 22.4). A solar activity related wind variation is obvious for altitudes above 90 km in summer with larger winds at high solar activity. The seasonal variation of zonal wind at 88 km is shown

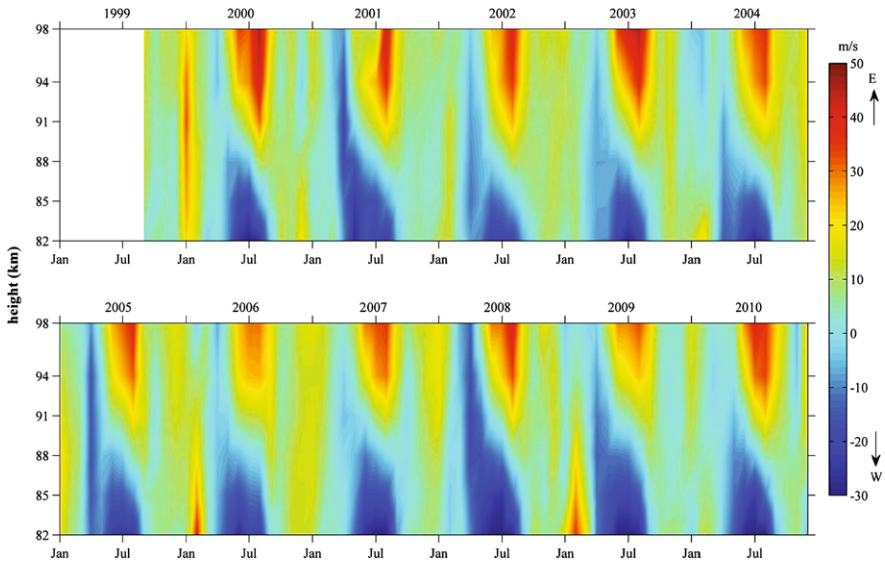


Fig. 22.2 Height-time cross section of zonal winds derived from Meteor radar measurements at Andenes and Kiruna between August 1999 and December 2010

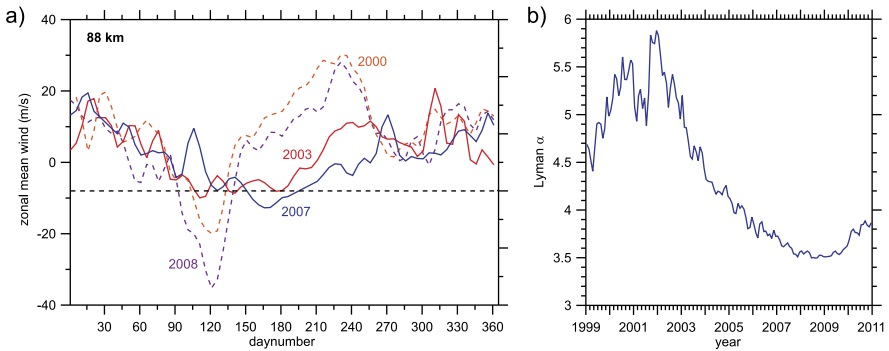


Fig. 22.3 (a) Seasonal variation of zonal winds at Andenes (69°N, *full lines*) for 2003 (enhanced solar activity) and 2007 (low solar activity) and at Juliusruh (55°N, *dashed lines*) for 2000 (solar maximum) and 2008 (solar minimum) at 88 km. Mean zonal wind from 10-day composite analyses are depicted. (b) Variation of the solar Lyman α radiation (units: $10^{11} \text{ ph. cm}^{-2} \text{ s}^{-1}$) between 1999 and 2010 basing on monthly mean values

for a year of enhanced solar activity (2003) and a year of low solar activity (2008) in Fig. 22.3a. Enhanced eastward winds are evident in summer 2003 (June, July, August) compared to summer at low solar activity whereas no clear signatures can be seen in winter. The solar activity varied during cycle 23 by a factor 1.7 between solar maximum and minimum as shown by the Lyman α radiation in Fig. 22.3b.

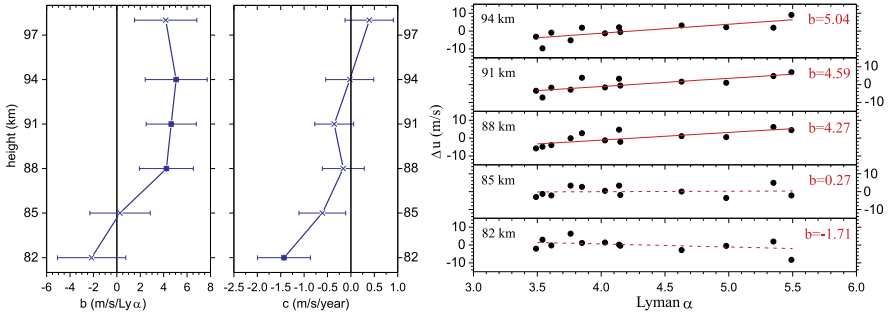


Fig. 22.4 (a) Height variation of the partial regression coefficients b and c (see Eq. (22.1)) between zonal wind at Andenes and solar activity (*left panel*) and the trend of zonal wind at Andenes (*right panel*) for summer (July, August). The significance level is marked by *full dots*, nonsignificant coefficients are marked by *crosses*. (b) Dependence of detrended zonal wind values on solar activity at altitudes between 82 km and 94 km. The significance level $\geq 95\%$ is characterized by *red full lines*, nonsignificant levels by *red dashed lines*. In addition, the regression coefficients b (corresponding to Fig. 22.4a) are added

Solar activity variations and trends of the MLT wind field are studied using robust regression [e.g. *Holland and Welsch, 1977; MATLAB, 2011*]. The robust fitting method is less sensitive than ordinary least squares to large changes in small parts of the data. The influence of the solar activity on the wind field and trends in the wind field are analyzed using the following twofold regression equation

$$u = a + b \times \text{Ly}\alpha + c \times \text{year}. \quad (22.1)$$

Regression analyses have been done separately for the zonal and meridional mean winds as well as for the tidal components at heights between 82 km and 98 km on the basis of seasonal median values. Summer median values are estimated from the results of harmonic analyses of 4-day composites shifted by one day covering July and August in total of 62 days. The most significant partial regression coefficients have been obtained for the zonal mean wind and summer conditions. The solar activity variation and a possible trend will be discussed in the following. Significantly increasing eastward directed winds are found between 88 km and 94 km with positive wind changes in the order of 4 to 5 m/s per Lyman α flux unit (Fig. 22.4a).

This value is in good agreement with the wind variations of about 5 to 10 m/s presented in Fig. 22.3a for summer 2003/2007 if we consider the corresponding solar activity variation by a factor of 1.3. The wind changes as a function of Lyman α flux are presented in Fig. 22.4b. A significant but small negative trend in zonal wind has been found only at 82 km with values around -1 m/s per year. This value agrees well with the results obtained at mid-latitudes from MF radar wind measurements at 3.18 MHz [Fig. 14 in *Keuer et al., 2007*]. Increasing eastward directed winds with increasing solar activity are found at high latitudes between 88 km and 94 km in comparison with decreasing eastward directed winds at mid-latitudes at 90 km and below [Fig. 7 in *Keuer et al., 2007*]. This difference is possibly related to the

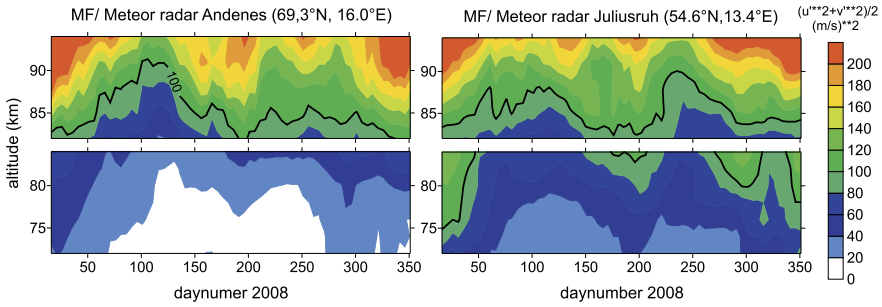


Fig. 22.5 Mean seasonal variations of GW kinetic energy derived from wind variances periods 3–9 hours from MF and meteor radar observations at Andenes (69°N) and Juliusruh (55°N) during 2008. Adopted in a modified form from *Hoffmann et al.* [2010]

different measurement techniques, as MF radars estimate smaller wind magnitudes above about 86 km–90 km compared to other techniques. Similar results are known from other investigations [for details see also *Hocking and Thayaparan, 1997; Manson et al., 2004; Jacobi et al., 2009; Engler et al., 2008*]. Meteor radar observations at Juliusruh during solar maximum (2000) and solar minimum (2008) showed a smaller increase of zonal winds with solar activity compared to the high-latitudes but the magnitudes at mid-latitudes are greater by a factor of about two (Fig. 22.3a). Nonsignificant solar activity variations and trends were found in the MF radar winds at 1.98 MHz at Andenes which are possibly related to the general weaker winds at high-latitudes and additionally influenced by the reduced MF radar winds above 84 km compared to other methods.

22.3.2 Annual and Latitudinal Variations of Gravity Waves

Continuous observations of mesospheric MF and Meteor radar winds allow the investigation of GW, first shown by *Manson and Meek [1986]*. In the following we use the kinetic energy derived by the sum of zonal and meridional wind variances divided by two as a measure of the GW activity. First, mean winds and tidal variations averaged over 7 days are removed from the hourly wind values to reduce the effects of background winds and tidal amplitudes on the GW activity. Then the variances for defined period bands are derived by wavelet transforms applying the Morlet mother wavelet of the 6-th order [for details see *Torrence and Compo, 1998; Serafimovich et al., 2005*]. A detailed description of the method applied to the data of one particular year is given in *Hoffmann et al. [2010]*. As an example, Fig. 22.5 shows the seasonal variation of the GW activity during 2008, as evaluated using the combined MF and meteor radar winds at Andenes and Juliusruh.

At both latitudes, the observations show a semi-annual variation with strongest GW energy during winter and a secondary maximum during summer. Minima of the GW activity appeared during the equinoxes at altitudes of about 90 km [*Hoffmann et*

al., 2010]. This semi-annual variation has been also found by the simulated annual cycle using the GW resolving version of the mechanistic general circulation model KMCM [for details of the model see *Becker, 2009*], and can be explained with the selective filtering of westward and eastward GWs by the mean zonal wind in the stratosphere and lower mesosphere following arguments of *Lindzen [1981]*. The latitudinal dependence during summer [for more details see *Hoffmann et al., 2010*, and Fig. 13 therein] is characterized by stronger GW energy below about 85 km at middle latitudes compared to at polar latitudes, and a corresponding upward shift of the wind reversal towards the pole. This is also reflected by the simulated GW drag. A possible explanation is the reduced westward flow in the polar summer stratosphere and lower mesosphere relative to middle latitudes, which results in a reduced filtering of westward propagating GWs and a stronger damping of eastward propagating waves.

22.3.3 Trends of Gravity Wave Activity

The seasonal variation of the GW activity as investigated in detail in [*Hoffmann et al. [2010]*] is based on radar data from one particular year and simulations with the KMCM. However, using all data derived from observations with the MF radar in Juliusruh from 1990–2010, the averaged annual cycle of GW activity [see *Hoffmann et al., 2011*, and Fig. 1b therein] confirms the semiannual variation with minima during the equinoxes, maxima during winter and slightly weaker during July/August. As mentioned above, the variability of the GW activity is generally assumed to be determined by the filtering due to the background winds in the stratosphere and lower mesosphere. Therefore, in *Hoffmann et al. [2011]* we investigated the following hypothesis: If there are trends in the background winds as e.g. shown by *Keuer et al. [2007]* using the Juliusruh-MF radar winds from 1990–2005, then these trends are considered to be responsible for long-term variations of gravity waves due to the filtering effect.

At first, we extended the trend analysis to the years 1990–2010. We found, as shown in Fig. 22.6a, stable negative trends of the zonal winds during summer, i.e., an enhancement of the westward directed summer jet, which dominates the seasonal variation during all years (see also Fig. 22.1). Using monthly mean values for July we found that the observed zonal wind trend at about 75 km goes along with an enhanced activity of GW with periods between 3–6 hours at altitudes above 80 km (Fig. 22.6b).

Indeed, also the year-to-year variation of maxima of the observed westward directed winds at altitudes near 75 km and the GW activity at about 80 km are significantly correlated (Fig. 22.6c) thus stimulating the further study of long-term wind changes and corresponding GW trends.

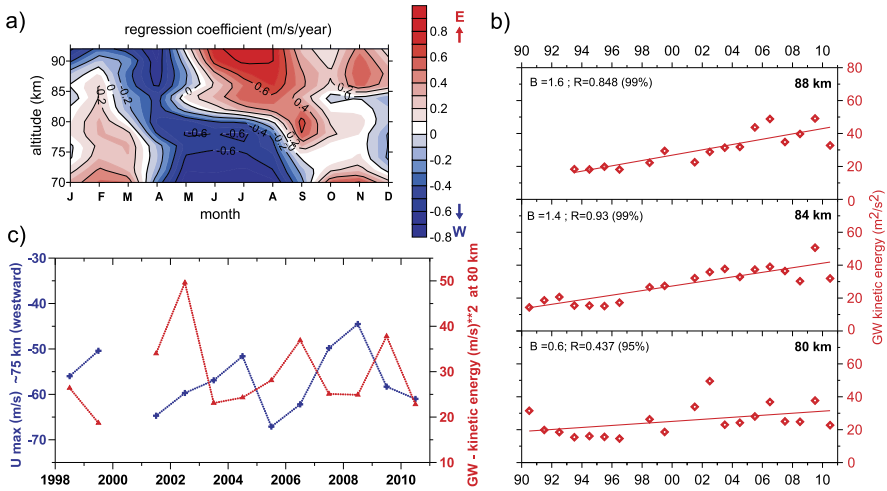


Fig. 22.6 (a) Mean height-time cross section of the trend in the zonal wind at Juliusruh from 1990–2010. (b) Trend of kinetic energy of GW (3–6 h) at Juliusruh at 80, 84 and 88 km for July. (c) Variation of GW—activity (kinetic energy, red line) at 80 km and westward directed jet strength (~75 km, blue line) during July at 55°N from 1998–2010 (no data during July 2000). Modified version of Figs. 2, 4, and 5 in *Hoffmann et al.* [2011]

22.4 Vertical Coupling During Sudden Stratospheric Warmings

22.4.1 Sudden Stratospheric Warmings in Winters 2006 and 2009

Continuous MF and meteor radar observations have been used for detailed studies of winds and temperatures in the upper mesosphere and lower thermosphere to understand the strong variability in winter 2006/07 due to enhanced planetary wave activity and related stratospheric warming events [*Hoffmann et al.*, 2007]. Such events are considered as an exceptionally striking vertical coupling process between lower, middle and upper atmosphere. It has been shown, that the strength of the observed zonal wind reversal in the mesosphere during SSW is decreasing with latitude. There are only weak longitudinal variations of zonal winds and temperatures at mesopause heights during major warmings but stronger longitudinal variations of meridional winds, as confirmed by comparisons to similar observations at Resolute Bay (75°N, 95°W) and Poker Flat (65°N, 147°W). The results during winter 1998/1999 and 2006/07 indicate the occurrence of a planetary wave 1 structure in the mesosphere. The short term reversals of the mesospheric winds during SSWs are followed by periods of intensified westerly winds connected with enhanced turbulent energy dissipation rates below 85 km, as estimated with the narrow beam Saura MF radar, and an increase of the gravity wave activity in the altitude range 70–85 km [more details about the winter 2006/2007 are given by *Hoffmann et al.*, 2007]. The seasonal variation of the gravity wave activity derived from the horizontal wind variability for periods between 3–9 hours and the turbulent energy dissipation rates in 2006 are

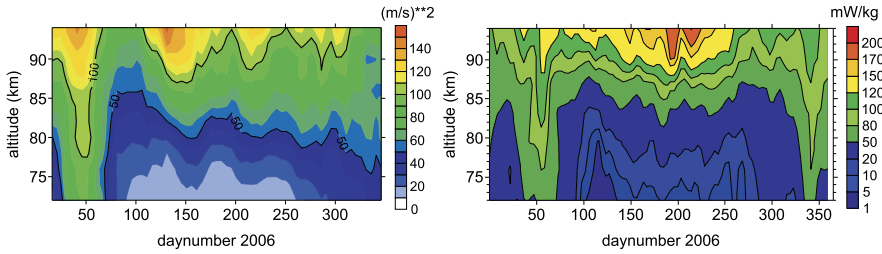


Fig. 22.7 Seasonal variation of horizontal wind variability for periods 3–9 hours (*left panel*) and seasonal variation of turbulent kinetic energy dissipation rate (*right panel*) over Andenes in 2006

shown in Fig. 22.7. Enhanced turbulent energy dissipation rates in February and in December go along with enhanced GW activity indicating that enhanced turbulence at that time is related to GW dissipation. In addition, the seasonal evolution and turbulence strength observed by the Saura MF radar is in general agreement with in situ measurements at Andenes [Lübken, 1997]. In February, the enhanced gravity wave activity and the intensified westerly winds are associated also with a period of reduced planetary wave 1 activity in the stratosphere [Hoffmann et al., 2007].

22.4.2 Major Stratospheric Warming 2009—Downwelling of NO

The major stratospheric warming in January 2009 is accompanied by a jump of the stratopause and its reformation at about 80 km in the first days of February as shown in (Fig. 22.8) by zonal averaged temperatures (0°E – 30°E) over Andenes from the Microwave Limb Sounder (MLS) instrument on the NASA-EOS Aura satellite [Livesey et al., 2007].

The stratopause returns to its normal level over a period of about six weeks. The observed cooling of the lower mesosphere is associated with forced propagation of eastward gravity waves during the enhanced zonal wind after wind reversal (see also Fig. 22.10). The major stratospheric warmings in winters 2004 and 2006 showed a similar behavior comparable to the descent of the stratopause in February 2009. Also von Zahn et al. [1998] observed a descent of an elevated stratopause by about 30 km in January/February 1998 with lidar observations at Andenes.

The descent of the stratopause to its normal level brings down minor constituents in the winter middle atmosphere which are present in the upper mesosphere/lower thermosphere. One important trace species of the lower thermosphere is nitric oxide NO which has a long life time in absence of sun light during the polar night. NO will be immediately ionized by solar UV at solar zenith distances less than about 98° under production of free electrons. The downwelling of nitric oxide has been studied using electron density as proxy measured with the Saura MF radar [Singer et al., 2011] as local ionization of nitric oxide by precipitating energetic particles should not happen under solar minimum conditions. Time series of electron density

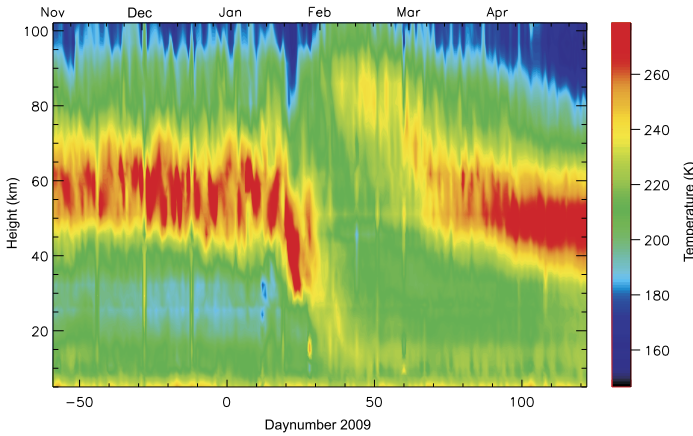


Fig. 22.8 MLS temperatures over Andenes (69°N, 16°E) around the major stratospheric warming in January 2009, a zonal average for the longitudes between 0°E and 30°E is shown. The stratospheric warming is accompanied by a jump of the stratopause and its reformation at about 80 km

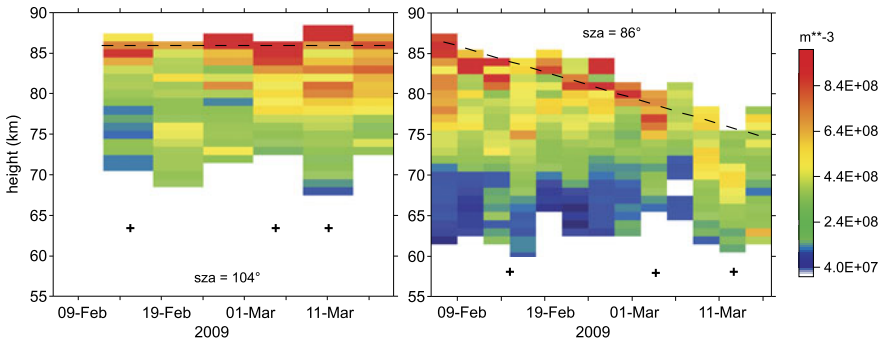
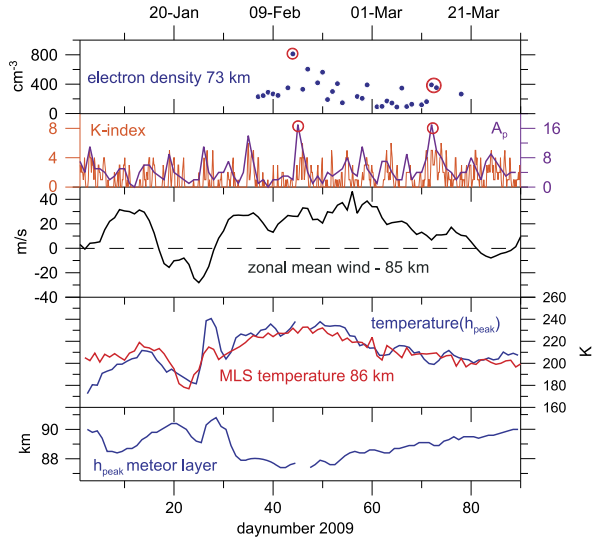


Fig. 22.9 Height-time cross-section of electron densities over Andenes at constant solar zenith angles (sza) 86° and 104° in February/March 2009 during the reformation phase of the stratopause after the stratospheric warming. The electron densities under sunlit conditions (sza = 86°) are descending with a rate of about 300 m/day whereas nearly constant electron densities are observed during night (sza = 104°) as indicated by *dashed lines*. The *crosses* mark geomagnetically disturbed periods with possibly direct production of NO_x by energetic particles (for details see text)

at constant solar zenith angles of 86° (sunlit conditions) and 104° (absence of sun light) were analyzed over periods of three days and six days, respectively due to the high background noise during polar night. Hight-time cross-sections of the observed electron densities for the period February 6 to March 17 are depicted in Fig. 22.9.

Under sunlit conditions (right panel) a descent of the electron peak density was found with a mean descent rate of about 300 m/day. During polar night a more or less constant height of peak electron density was estimated (Fig. 22.9, left panel). In both cases excursions are observed which are marked by crosses which are possibly

Fig. 22.10 Mesospheric electron density at 73 km during local noon, global geomagnetic activity A_p and 3-hourly K-index from Tromsø, mean zonal wind at 85 km prior, during, and after the stratospheric warming event, mesopause temperatures from MLS measurements and meteor decay times, and peak height of the meteor layer for the period January to March 2009. The red circles indicate minor geomagnetic storms



related to the direct ionization of nitric oxide by precipitating energetic particles from aurora or from the radiation belts. The variation of the global geomagnetic index A_p (Fig. 22.10) and the variation of the 3-hourly K index with values equal or greater five indicates the occurrence of minor geomagnetic storms on February 4 and 14/15 and on March 4 and 13/14 in agreement with the observed electron density excursions.

The descent rate of day-time electron density of ~ 300 m/day is not so different from the NO_x descent rate of about 700 m/day obtained by *Salmi et al.* [2011] from a chemistry transport model (3-D FinRose) in connection with ACE-FTS (Atmospheric Chemistry Experiment Fourier Transform Spectrometer) observations in February/March 2009. WACCM simulations by *Smith et al.* [2011] showed that the wave driven mean circulation is the dominating transport process bring down trace species in the winter middle atmosphere. The downwelling phase in February is accompanied with a cooling and shrinking of the middle atmosphere which is also reflected by a lowering of the peak height of the meteor layer during that time as the meteoroids descending on the upper atmosphere with the same entry velocities burn up at the same pressure level (lowest panel of Fig. 22.10). In addition, the neutral temperatures derived from meteor decay times at the peak height of the meteor layer agree well with the temperatures from MLS measurements at 86 km in magnitude and temporal evolution.

22.5 Mesospheric Response on Solar Activity Storms

During solar proton events (SPE) large fluxes of energetic protons impacted the mesosphere and stratosphere causing ionization, dissociation, and excitation. Drastic changes of the ionospheric plasma with excessive ionization enhancements down

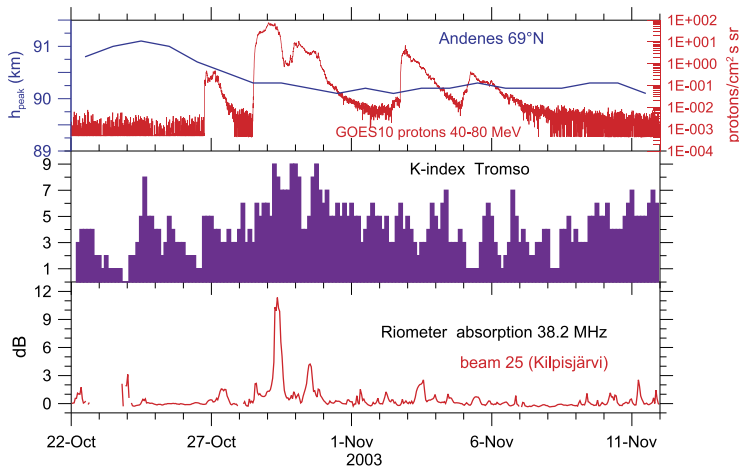


Fig. 22.11 Solar proton events in October/November 2003: solar proton fluxes with energies 40–80 MeV from GOES 10 observations and variation of the peak height of the meteor layer, geomagnetic activity expressed by the 3-hourly K-index from Tromso indicating severe geomagnetic storms ($K = 9$) after October 28, and ionospheric radio wave absorption of the imaging riometer at Kilpisjärvi (beam 25 sampled the ionosphere over Andenes)

to altitudes of 60 km are well known against it measurements of dynamical and structural changes during these perturbations are rare. The MF radar and meteor radar observations at Andenes (69°N) and Juliusruh (55°N) have been used to study the influence of the strongest four SPEs on the MLT dynamics occurring during the last decade. These SPE events appeared in July 2000 (24000 pfu), October 2003 (29500 pfu), January 2005 (5040 pfu), and December 2006 (1980 pfu), the values in brackets characterize the strength of the event through the proton flux with energies greater than 10 MeV: $1 \text{ pfu} = 1 \text{ protons/cm}^2 \text{ s}^{-1} \text{ sr}$. Special emphasis is given to the observations during the strongest SPE in October 2003 as *Jackman et al. [2007]* used the Thermosphere Ionosphere Mesosphere Electrodynamics General Circulation Model (TIME-GCM) to study the mesospheric changes induced by the October 2003 event.

The interactions of protons with air molecules and trace species resulted in the production of odd hydrogen and odd nitrogen. The enhancements of these constituents lead to a destruction of ozone via catalytic cycles resulting in a cooling of the lower mesosphere below about 80 km due to reduced ozone heating. A weak temperature increase was found above 80 km peaking around 95 km. The Joule heating rates were much less than the solar/chemical heating rates. Temperature changes up to $\pm 2.6 \text{ K}$ and wind changes up to 20–25 % were obtained whereas the largest response was located in the sunlit southern hemisphere.

MF and meteor radar winds cover the height range between 70 and 94 km during the October 2003 SPE on the northern winter hemisphere. The proton event started on October 28 and reached its maximum on October 29, the geomagnetic field over northern Scandinavia was severely disturbed from October 29 onward

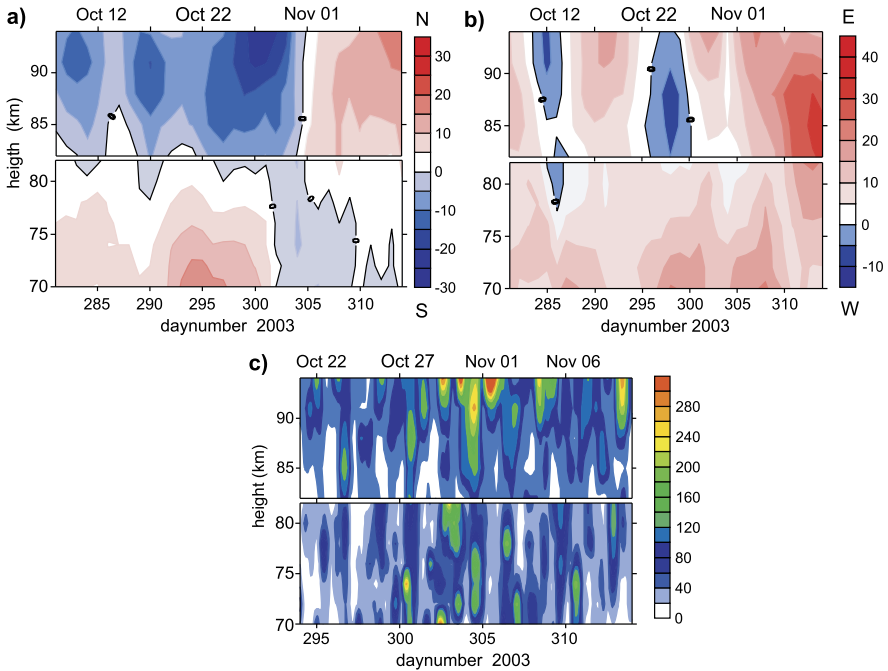


Fig. 22.12 MF/meteor radar observations during the SPEs in October/November 2003: (a) mean meridional winds, (b) mean zonal winds, (c) variances of horizontal wind disturbances for periods 3–9 hours

causing additional ionization due to precipitation energetic particles from the radiation belts indicated by the excessive riometer absorption over Andenes (Fig. 22.11). In addition, the peak altitude of the meteor layer was decreasing during the SPE by up to about 1 km indicating a cooling and shrinking of the lower mesosphere below. At the maximum of the event on October 29 (day 302) and a few days later a reversal of the meridional winds from equatorwards to polewards was observed above 82 km and the opposite situation below that altitude. At same time the zonal winds are increasing above about 80 km and below 78 km (Fig. 22.12).

The increase of eastward directed winds is associated with enhanced GW activity at these altitudes and above as eastward propagating GWs can dissipate at lower altitudes (Fig. 22.12c).

An increase of the eastward directed zonal mean winds has been observed above 85 km for all SPEs studied here (Fig. 22.13). Below 85 km a positive zonal wind response was found only in winter whereas no significant differences (less than 2–5 m/s) between undisturbed and disturbed wind fields appeared in summer and autumn. *Becker and von Savigny [2010]* studied the mesospheric response on an SPE during summer using a mechanistic general circulation model. They found that the temporary ozone reduction during an SPE results in an positive zonal wind response between 70 km and about 95 km in the order of 2–8 m/s what is in general agreement with our observations during the July 2000 event.

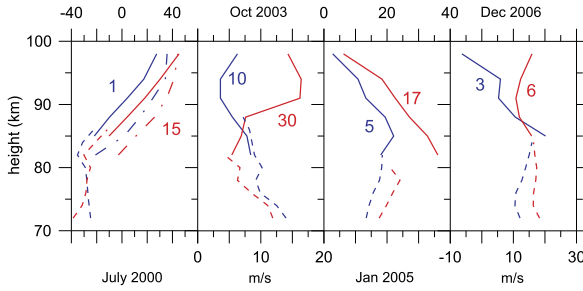


Fig. 22.13 Zonal mean winds (m/s) before the solar proton events (*blue lines*) and at the maximum phase (*red lines*) of the events in July 2000, October 2003, January 2005, and December 2006. Meteor radar observations at Andenes/Kiruna (*full lines*) and Juliusruh (*dashed-dotted lines*) as well as MF radar (*dashed lines*) observations are depicted (the figures indicate the corresponding days, note the different scales for summer and winter)

22.6 Summary

Long-term wind measurements by MF and meteor radars at high and middle latitudes from 1990 to 2011 provide reliable data to study trends and apparent solar activity related variations of the wind field between about 70 km and 95 km during the measurement period. Significant trends with time and with solar activity are found for the zonal wind preferred in summer. At mid-latitudes a negative zonal wind response (decreasing strength of eastward winds) with time was found below about 82 km from MF radar observations whereas at high latitudes a negative zonal wind response was determined in a height of 82 km from meteor radar observations in the same order of about -1 m/s per year. A significant variation with solar activity was observed at high latitudes in summer (July and August of the years 2000 to 2011) at altitudes above 85 km with a positive zonal wind response (increasing strength of eastward winds) in the order of 4 to 5 m/s per Lyman α flux unit. That is a first indication of an apparent solar activity induced wind variation but longer time series are required to verify the finding. Keuer *et al.* [2007] obtained from MF radar measurements at mid-latitudes for summer (April to September, 1990 to 2005) a negative zonal wind response in the order of about 5 m/s per Lyman α flux unit for altitudes below 90 km. In addition, a general positive zonal wind response was found during the strongest solar proton events occurred between 2000 and 2006 for altitudes above 85 km. No significant changes between disturbed and undisturbed conditions have been seen below 85 km. The strong response of the upper mesosphere on severe solar activity storms during all seasons indicates that also high levels of solar UV radiation can possibly induce changes of the wind field above 85 km as found at high latitudes for the period 2000 to 2011. A possible mechanism effecting the wind field at altitudes below 85 km can be related to the influence of the global warming effect on the mesospheric circulation. Changes of the zonal wind field obtained with the Hamburg Model of the Neutral and Ionized Atmosphere (HAMMONIA) for doubling the CO₂ content show qualitatively the same behavior of a decreasing strength of eastward winds below 83 km in summer and increasing eastward winds

above 83 km [Schmidt *et al.*, 2006]. The analysis of 12 years of observations provides some evidence of possible trends and solar activity related variations of the mesospheric wind field but at least 10 years more observations are needed to verify the result.

The wind measurements have been used to study the seasonal and inter-annual variations of GW at high and middle northern latitudes. The annual cycle of the GW activity is characterized by a semi-annual variation with a stronger maximum in winter and a weaker in summer consistent with the selective filtering of westward and eastward propagating GWs by the mean zonal wind. Long-term changes of the background winds influence the activity of upward propagating GWs at mid-latitudes. The most significant long-term trend of zonal wind at about 75 km during July goes along with an enhanced activity of GWs with periods of 3 to 6 hours at altitudes between 80 km and 88 km. The direct relation between the maxima of the westward directed winds at altitudes near 75 km and the enhanced GW activity at about 80 km shows a significant anticorrelation and stimulates further studies of long-term wind changes and corresponding GW trends.

The mesospheric response on major sudden stratospheric warmings and on solar proton events looks quite similar. After SSWs and SPEs in winter a general increase of the eastward directed winds associated with mesospheric coolings and an increase of turbulence are observed but the reasons are different. Gravity waves play an important role in the coupling during SSWs as the mesospheric coolings associated with SSWs are intensified by improved propagation of eastward directed gravity waves due to enlarged eastward background winds. The mesospheric coolings and related wind changes after SPEs result from reduced ozone heating due to ozone destruction by energetic protons.

Acknowledgements The authors are grateful to Erich Becker and Markus Rapp for their support and helpful discussions. We also thank Ralph Latteck and Dieter Keuer for their support running the radars at Andenes and Juliusruh. This work has been supported by DFG in the frame of the CAWSES priority program SPP 1176 under grants SI 501/5-1 and SI 501/5-2. We thank the Jet Propulsion Laboratory/NASA for providing data access to the Aura/MLS level 2.2 retrieval product. The data originated from the Imaging Riometer for Ionospheric Studies (IRIS), operated by the Space Plasma Environment and Radio Science (SPEARS) group, Department of Physics, Lancaster University (UK) in collaboration with the Sodankylä Geophysical Observatory.

References

- Becker, E. (2009). Sensitivity of the upper mesosphere to the Lorenz energy cycle of the troposphere. *Journal of the Atmospheric Sciences*, 66, 647–666.
- Becker, E., & von Savigny, C. (2010). Dynamical heating of the polar summer mesopause by solar proton events. *Journal of Geophysical Research*, 115, D00I18. doi:[10.1029/2009JD012,561](https://doi.org/10.1029/2009JD012,561).
- Briggs, B. (1984). The analysis of spaced sensor records by correlation techniques. In R. Vincent (Ed.), *Handbook for MAP: Vol. 13. Middle atmosphere program* (pp. 166–186). SCOSTEP.
- Burrage, M. D., Skinner, W. R., Gell, D. A., Hays, P. B., Marshall, A. R., Ortlund, D. A., Manson, A. H., Franke, S. J., Fritts, D. C., Hoffmann, P., McLandress, C., Niciejewski, R., Schmidlin, F. J., Shepherd, G. G., Singer, W., Tsuda, T., & Vincent, R. A. (1996). Validation of mesosphere

- and lower thermosphere winds from the high resolution Doppler imager on UARS. *Journal of Geophysical Research*, 101(D6), 10365–10392. doi:[10.1029/95JD01700](https://doi.org/10.1029/95JD01700).
- Engler, N., Singer, W., Latteck, R., & Strelnikov, B. (2008). Comparison of wind measurements in the troposphere and mesosphere by VHF/MF radars and in-situ techniques. *Annales Geophysicae*, 26, 3693–3705.
- Fritts, D. C. (1984). Gravity wave saturation in the middle atmosphere: a review of theory and observations. *Reviews of Geophysics and Space Physics*, 22, 275–308.
- Fritts, D. C., & Alexander, M. J. (2003). Gravity wave dynamics and effects in the middle atmosphere. *Reviews of Geophysics*, 41(1), 1003. doi:[10.1029/2001RG000106](https://doi.org/10.1029/2001RG000106).
- Fritts, D. C., & Nastrom, G. D. (1992). Sources of mesoscale variability of gravity waves. Part II: frontal, convective, and jet stream excitation. *Journal of the Atmospheric Sciences*, 49, 111–127.
- Fritts, D. C., Vadas, S. L., Wan, K., & Werne, J. A. (2006). Mean and variable forcing of the middle atmosphere by gravity waves. *Journal of Atmospheric and Solar-Terrestrial Physics*, 68, 247–265.
- Hines, C. O. (1960). Internal atmospheric gravity waves at ionospheric heights. *Canadian Journal of Physics*, 38, 1441–1481.
- Hocking, W. K., & Thayaparan, T. (1997). Simultaneous and colocated observation of winds and tides by MF and meteor radars over London, Canada (43°N, 81°W), during 1994–1996. *Radio Science*, 32(2), 833–865. doi:[10.1029/96RS03467](https://doi.org/10.1029/96RS03467).
- Hocking, W. K., Fuller, B., & Vandepeer, B. (2001). Real-time determination of meteor-related parameters utilizing modern digital technology. *Journal of Atmospheric and Solar-Terrestrial Physics*, 63, 155–169.
- Hocking, W. K., Singer, W., Bremer, J., Mitchell, N. J., Batista, P., Clemensha, B., & Donner, M. (2004). Meteor radar temperatures at multiple sites derived with SKiMET radars and compared to OH, rocket and lidar measurements. *Journal of Atmospheric and Solar-Terrestrial Physics*, 66, 585–593.
- Hoffmann, P., Singer, W., Keuer, D., Hocking, W. K., Kunze, M., & Murayama, Y. (2007). Latitudinal and longitudinal variability of mesospheric winds and temperatures during stratospheric warming events. *Journal of Atmospheric and Solar-Terrestrial Physics*, 69(17–18), 2355–2366. doi:[10.1016/j.jastp.2007.06.010](https://doi.org/10.1016/j.jastp.2007.06.010).
- Hoffmann, P., Becker, E., Singer, W., & Placke, M. (2010). Seasonal variation of mesospheric waves at northern middle and high latitudes. *Journal of Atmospheric and Solar-Terrestrial Physics*, 72(14–15), 1068–1079. doi:[10.1016/j.jastp.2010.07.002](https://doi.org/10.1016/j.jastp.2010.07.002).
- Hoffmann, P., Rapp, M., Singer, W., & Keuer, D. (2011). Trends of mesospheric gravity waves at northern middle latitudes during summer. *Journal of Geophysical Research*, 116, D00P08. doi:[10.1029/2011JD015717](https://doi.org/10.1029/2011JD015717).
- Holland, P. W., & Welsch, R. (1977). Robust regression using iteratively reweighted least squares. *Communications in Statistics. Theory and Methods*, A6, 813–827.
- Jackman, C. H., Roble, R. G., & Fleming, E. L. (2007). Mesospheric dynamical changes induced by the solar proton events in October–November 2003. *Geophysical Research Letters*, 34, L04812. doi:[10.1029/2006GL028328](https://doi.org/10.1029/2006GL028328).
- Jacobi, C., Arras, C., Kürschner, D., Singer, W., Hoffmann, P., & Keuer, D. (2009). Comparison of mesopause region meteor radar winds, medium frequency radar winds and low frequency drifts over Germany. *Advances in Space Research*, 43, 247–252. doi:[10.1016/j.asr.2008.05.009](https://doi.org/10.1016/j.asr.2008.05.009).
- Keuer, D., Hoffmann, P., Singer, W., & Bremer, J. (2007). Long-term variations of the mesospheric wind field at mid-latitudes. *Annales Geophysicae*, 25(8), 1779–1790.
- Latteck, R., Singer, W., & Hocking, W. K. (2005). Measurement of turbulent kinetic energy dissipation rates in the mesosphere by a 3 MHz Doppler radar. *Advances in Space Research*, 35(11), 1905–1910.
- Lindzen, R. S. (1981). Turbulence and stress owing to gravity wave and tidal breakdown. *Journal of Geophysical Research*, 86, 9707–9714.
- Livesey, N. J., Read, W. G., Lambert, A., Cofield, R. E., Cuddy, D. T., Froidevaux, L., Fuller, R. A., Jarnot, R. F., Jiang, J. H., Jiang, Y. B., Knosp, B. W., Kovalenko, L. J., Pickett, H. M.,

- Pumphrey, H. C., Santee, M. L., Schwartz, M. J., Stek, P. C., Wagner, P. A., Waters, J. W., & Wu, D. L. (2007). *EOS MLS version 2.2 level 2 data quality and description document* (Technical Report, Version 2.2 D-33509). Jet Propulsion Lab., California Institute of Technology, Pasadena, California, 91198-8099.
- Lübken, F.-J. (1997). Seasonal variation of turbulent energy dissipation rates at high latitudes as determined by in situ measurements of neutral density fluctuations. *Journal of Geophysical Research*, *102*, 13441–13456.
- Manson, A. H., & Meek, C. E. (1986). Dynamics of the middle atmosphere at Saskatoon (52°N, 107°W): a spectral study during 1981, 1982. *Journal of Atmospheric and Solar-Terrestrial Physics*, *48*, 1039–1055.
- Manson, A. H., Meek, C. E., Hall, C. M., Nozawa, S., Mitchell, N. J., Pancheva, D., Singer, W., & Hoffmann, P. (2004). Mesopause dynamics from the Scandinavian triangle of radars within the PSMOS-DATAR project. *Annales Geophysicae*, *22*, 367–386.
- MATLAB (2011). Toolbox statistics. www.mathworks.de.
- Mitchell, N., Pancheva, D., Middleton, H., & Hagan, M. (2002). Mean winds and tides in the arctic mesosphere and lower thermosphere. *J. Geophys. Res.*, *107*. doi:10.1029/2001JA900127.
- Nastrom, G. D., & Fritts, D. C. (1992). Sources of mesoscale variability of gravity waves. I: topographic excitation. *Journal of the Atmospheric Sciences*, *49*, 101–110.
- Pancheva, D., Singer, W., & Mukhtarov, P. (2007). Regional response of the mesosphere-lower thermosphere dynamics over Scandinavia to solar proton events and geomagnetic storms in late October 2003. *Journal of Atmospheric and Solar-Terrestrial Physics*, *69*, 1075–1094. doi:10.1016/j.jastp.2007.04.005.
- Salmi, S.-M., Verronen, P. T., Thölix, L., Kyrölä, E., Backman, L., Karpechko, A. Y., & Seppälä, A. (2011). Mesosphere-to-stratosphere descent of odd nitrogen in early 2009 after a major stratospheric warming. In *3rd workshop on high energy particle precipitation in the atmosphere*, Granada, Spain, 9–11 May.
- Schmidt, H., Brasseur, G. P., Charron, M., Manzini, E., Giorgetta, M. A., Diehl, T., Fomichev, V. I., Kinnison, D., Marsh, D., & Walters, S. (2006). The HAMMONIA chemistry climate model: sensitivity of the mesopause region to the 11-year solar cycle and CO₂ doubling. *Journal of Climate*, *19*(16), 3903–3931. doi:10.1175/JCLI3829.1.
- Serafimovich, A., Hoffmann, P., Peters, D., & Lehmann, V. (2005). Investigation of inertia-gravity waves in the upper troposphere/lower stratosphere over Northern Germany observed with collocated VHF/UHF radars. *Atmospheric Chemistry and Physics*, *5*, 295–310.
- Singer, W., Keuer, D., & Eriksen, W. (1997). The ALOMAR MF radar: technical design and first results. In B. Kaldeich-Schürmann (Ed.), *Proceedings 13th ESA symposium on European rocket and balloon programmes and related research*, Oeland, Sweden, 26–29 May 1997 (ESA SP-397) (pp. 101–103). ESA Publications Division.
- Singer, W., Bremer, J., Hocking, W. K., Weiss, J., Latteck, R., & Zecha, M. (2003). Temperature and wind tides around the summer mesopause at middle and arctic latitudes. *Advances in Space Research*, *31*(9), 2055–2060.
- Singer, W., Bremer, J., Weiss, J., Hocking, W. K., Höffner, J., Donner, M., & Espy, P. (2004). Meteor radar observations at middle and arctic latitudes, part 1: mean temperatures. *Journal of Atmospheric and Solar-Terrestrial Physics*, *66*, 607–616.
- Singer, W., Latteck, R., Hoffmann, P., Williams, B. P., Fritts, D. C., Murayama, Y., & Sakanoi, K. (2005). Tides near the Arctic summer mesopause during the MaCWAVE/MIDAS summer program. *Geophysical Research Letters*, *32*, L07S90. doi:10.1029/2004GL021607.
- Singer, W., Latteck, R., & Holdsworth, D. (2008). A new narrow beam Doppler Radar at 3 MHz for studies of the high-latitude middle atmosphere. *Advances in Space Research*, *41*, 1487–1493. doi:10.1016/j.asr.2007.10.006.
- Singer, W., Latteck, R., Friedrich, M., Wakabayashi, M., & Rapp, M. (2011). Seasonal and solar activity variability of D-region electron density at 69°N. *Journal of Atmospheric and Solar-Terrestrial Physics*, *73*, 925–935.
- Smith, A. K., Garcia, R., Marsh, D., & Richter, J. (2011). WACCM simulations of the mean circulation and trace species transport in the winter mesosphere. *Journal of Geophysical Research*,

116, D20115. doi:[10.1029/2011JD016083](https://doi.org/10.1029/2011JD016083).

- Torrence, C., & Compo, G. P. (1998). A practical guide to wavelet analysis. *Bulletin of the American Meteorological Society*, 79(1), 61–78.
- Vincent, R. A., & Alexander, M. J. (2000). Gravity waves in the tropical lower stratosphere: an observational study of seasonal and interannual variability. *Journal of Geophysical Research*, 105, 17971–17982.
- von Zahn, U., Fiedler, J., Naujokat, B., Langematz, U., & Krüger, K. (1998). A note on record-high temperatures at the northern polar stratopause in winter 1997/98. *Geophysical Research Letters*, 25, 4169–4172.
- Ward, W. E., Oberheide, J., Goncharenko, L. P., Nakamura, T., Hoffmann, P., Singer, W., Chang, L. C., Du, J., Wang, D.-Y., Batista, P., Clemesha, B., Manson, A. H., Riggini, D. M., She, C.-Y., Tsuda, T., & Yuan, T. (2010). On the consistency of model, ground-based, and satellite observations of tidal signatures: initial results from the CAWSES tidal campaigns. *Journal of Geophysical Research*, D115, D07107. doi:[10.1029/2009JD012593](https://doi.org/10.1029/2009JD012593).
- Weatherhead, E. C., Reinsel, G., Tiao, G., Meng, X.-L., Choi, D., Cheang, W.-K., Keller, T., DeLuisi, J., Wuebbles, D., Kerr, J., Miller, A., Oltmans, S., & Frederick, J. (1998). Factors affecting the detection of trends: statistical considerations and applications to environmental data. *Journal of Geophysical Research*, 103(D14), 17149–17161.